J Comput Electron (2014) 13:313–322
DOI 10.1007/s10825-013-0529-9

Numerical study of the effect of defect layer on unmagnetized plasma photonic crystals

Tony W.H. Sheu · R.Y. Chang · Y.W. Chang · J.H. Li

Published online: 12 November 2013

Abstract In this paper an explicit finite-difference time domain scheme developed in staggered grids is used to solve the Maxwell's equations in Drude medium. Besides the preservation of discrete zero-divergence condition in electric and magnetic fields, we also aim to conserve the inherent conservation laws in simple medium all the time using the temporally second-order accurate explicit symplectic partitioned Runge-Kutta scheme. Within the framework of a semidiscretized method, the first-order spatial derivative terms in Faraday's and Ampère's equations are approximated to get an accurate numerical dispersion relation equation. The derived numerical angular frequency is accurately related to the wavenumber of Maxwell's equations for the space centered scheme of fourth-order accuracy. The resulting symplectic finite difference scheme developed in the time domain minimizes the difference between the exact and numerical group velocities. This newly proposed scheme is applied to model EM waves in the unmagnetized plasma crystal which contains a defect layer in photonic crystal. Our purpose is to numerically study the effects of defect layers on the propagation insight.

Keywords Maxwell's equations · Drude medium · Symplectic partitioned Runge-Kutta · Dispersion relation equation · Numerical group velocity

T.W.H. Sheu (✉) · R.Y. Chang · Y.W. Chang · J.H. Li
Department of Engineering Science and Ocean Engineering, National Taiwan University, No. 1, Sec. 4, Roosevelt Road, Taipei, Taiwan
e-mail: twhsheu@ntu.edu.tw

1 Introduction

Maxwell's equations in vacuum have a geometric symplectic structure. Numerical simulation of these equations should discretely preserve their mathematically embedded Hamiltonians and Casimirs at all times [1]. In the absence of discrete symplecticity, design of a long-range high-quality optical device by numerical methods is at risk. Approximation of the first-order spatial derivative terms is required to avoid yielding larger numerical dispersion error. Otherwise, the introduced error of the dispersive type can produce a poorly predicted propagation speed and, as a result, may further generate unphysically oscillatory solution. Beside the error generated in the approximation of time and space derivative terms, numerical simulation of Ampère's and Faraday's equations is constrained to satisfy Gauss's law in discrete context [2]. These theoretical considerations have prompted scheme development to be aimed at preserving dispersion-relation equation, enforcing divergence-free conditions for electric and magnetic fields, and conserving symplecticity in non-staggered (or colocated) grids.

Our previously developed scheme [3] will be extended in this study to solve the Maxwell's equations for the frequency-dependent Drude medium. Instead of minimizing the numerical modified wavenumber derived in [3, 4], the difference between the numerical and exact group velocities is minimized in this study for achieving the goal of rigorously relating the time increment to the grid spacing while solving the transverse magnetic (TM) wave equations. The need of deriving the numerical dispersion relation equation by minimizing the dispersive errors of different kinds motivates the use of the explicit partitioned Runge-Kutta (PRK) non-iterative scheme [4] rather than the implicit Runge-Kutta symplectic scheme applied earlier in [3]. In addition, the classical Yee's staggered grid approach [5] is adopted

in this study. In [3] and [4], the less explored non-staggered grid approach was employed for the satisfaction of discrete Gauss law.

To avoid the unphysical wave reflection from a truncated boundary, we can either prescribe a proper radiation condition along the truncated boundary or attach a layer of finite width to a region immediately adjacent to the truncated boundary. The well known CPML (Convolutional Perfectly Matched Layer) approach of Roden [6] is employed in this study to effectively absorb reflected waves.

While performing numerical simulation in time domain, one can adopt explicit or implicit schemes. The unconditionally stable implicit scheme has the advantage of allowing use of a larger time step while solving Maxwell's equations. On the other hand, use of the implicit type time integrator requires an expensive matrix calculation, possibly requiring considerable memory storage. The computational cost can be large, in particular for a three-dimensional EM wave simulation. To circumvent these difficulties using an implicit scheme without the constraints imposed on the Courant stability condition, the alternating direction implicit (ADI) technique [7] and the concept of factorization-splitting [8] can be applied to reduce the matrix size. The consequence is that calculation of Maxwell's equations becomes computationally much less intensive.

In this study we aim to get a dispersively more accurate solution through the optimization of the numerical group velocity of the EM wave. As a result, an explicit method needs to be adopted so as to be able to get the explicit expression for the numerical dispersion relation equation. One can refer to [9] for a comprehensive review of the time-domain methods applied for solving the Maxwell's equations.

In periodic optical structures, electromagnetic waves with a specific wavelength cannot propagate in photonic crystals because of the possible strong scattering effect, thereby leading to the formation of bandgaps in photonic crystals. Bandgap is a forbidden energy zone where EM waves can not be transmitted through the material. Like the defect state generated in the forbidden band in doped semiconductors, defect layers can be also added to photonic crystals to break their spatial periodicity. Under some circumstances, this can decrease, therefore, producing a strong scattering effect. This phenomenon in photonic bandgaps is investigated in this study under different defect conditions. Four conditions, namely, the dielectric constant of the defect layer, the location of the defect layer, the number of periods for the periodic bilayer, and the width of the defect layer can very often affect the defect mode in plasma photonic crystals. They will be studied in terms of the transmission coefficient.

The rest of this paper is organized as follows. In Sect. 2, Maxwell's equations applicable to simulation of EM waves in non-dispersive and dispersive media are presented in free space as well as in perfectly matched layers. A splitting solution algorithm is applied to the ideal Maxwell equations. These lossless equations can then be rigorously approximated not only in space but also in time. In Sect. 4, the explicit PRK symplectic temporal scheme developed to conserve the Hamiltonian for the ideal Maxwell equations is applied. Employment of this non-iterative explicit scheme enables us to derive the numerical dispersion relation equation. In Sect. 5 development of the scheme which is featured with optimized numerical group velocities are detailed. We first analytically verify the proposed numerical method. This is followed by discussion of the results predicted in the investigated Drude medium in Sect. 6. Finally, some concluding remarks are drawn in Sect. 7.

2 Working equations

The dispersive medium permittivity and permeability in dispersive media are, as usual, functions of optical frequency. In the current numerical study, in the time domain, only the electric permittivity is assumed to be frequency-dependent for simplicity. The electric permittivity $\epsilon(t)$ $(\equiv \epsilon_r \epsilon_o)$ is equal to $(1+\chi)\epsilon_0$, where ϵ_r $(\equiv 1+\chi)$ is the relative permittivity, $\chi(t)$ the electric susceptibility, t the time, and ϵ_0 the vacuum permittivity.

For a dispersive medium whose magnetic permeability is frequency independent, the Ampère's and Faraday's laws respectively are represented below in time domain for the electric field variable $\underline{E}$ and the magnetic field variable $\underline{H}$

$$\frac{\partial}{\partial t}\big(\epsilon(\underline{x},t) * \underline{E}(\underline{x},t)\big) = \nabla \times \underline{H} - \underline{J}_d, \tag{1}$$

$$\mu \frac{\partial \underline{H}}{\partial t} = -\nabla \times \underline{E}. \tag{2}$$

In Eq. (2), μ is identical to $\mu_0 \mu_r$. The optical properties μ_0 and μ_r represent the free-space magnetic permeability and the relative magnetic permeability respectively. The polarization current $\underline{J}_d$ shown in (1) varies with the dispersive optical medium under investigation. For simplicity, both of the volume electric and magnetic current densities are assumed to be zero under the source-free condition. The resulting differential system is solved subject to Gauss's equations $\nabla \cdot \underline{B} = \nabla \cdot \underline{D} = 0$ in the context of electromagnetic equations. The notation "$*$" in Eq. (1) denotes the convolutional operator, defined as $f(t) * g(t) = \int_0^t f(t-\tau) g(\tau)\, d\tau$ for arbitrary functions $f(t)$ and $g(t)$.

Three constitutive models, namely, the Debye, Drude and Lorentz dispersive media have been frequently employed in electromagnetic wave simulation. The susceptibility functions $\chi(\omega)$ for these media vary with time t and frequency ω.

The vector equation used for modeling the polarization current is given below for the currently investigated Drude dispersive medium

$$\gamma_p \frac{\partial \underline{J}_d}{\partial t} + \frac{\partial^2 \underline{J}_d}{\partial t^2} = \epsilon_0 \omega_p^2 \frac{\partial \underline{E}}{\partial t}. \tag{3}$$

In the above, ω_p ($\equiv 2\pi f_p$) is the Drude pole frequency of the medium. The inverse of the pole relaxation time is denoted as γ_p ($\equiv$ 20 GHz). The susceptibility and the relative electric permittivity are given as $\chi(\omega) = -\frac{\omega_p^2}{\omega^2 - j\omega\gamma_p}$, $\chi(t) = \frac{\omega_p^2}{\gamma_p}(1 - e^{-\gamma_p t})u(t)$ and $\epsilon_r(\omega) = \epsilon_\infty - \frac{\omega_p^2}{\omega^2 - j\omega\gamma_p}$.

When simulating electromagnetic wave propagation, the analysis domain must be truncated. Truncation of the physical domain can unfortunately lead to reflection of waves from the truncated boundary if not carefully treated. If a wave re-enters the domain of interest, the numerically generated wave will interact with incident waves. To reduce the unphysical reflection from truncated boundaries, one can prescribe a proper set of differential equations along the truncated boundary or attach a finite width layer to absorb reflected waves. A convolutional perfectly matched layer is attached to the truncated boundary in this study.

The TM-mode Maxwell equations in the convolutional perfectly matched layer (CPML) are recast as follows in the time domain [6]

$$\begin{aligned}
\frac{\partial E_z}{\partial t} &= \frac{1}{\epsilon_0 \epsilon_r}\left(\frac{1}{k_x}\frac{\partial H_y}{\partial x} - \frac{1}{k_y}\frac{\partial H_x}{\partial y} - \underline{J}_{d,z} + \psi_{E_{z,x}} - \psi_{E_{z,y}}\right),\\
\frac{\partial H_x}{\partial t} &= -\frac{1}{\mu_0 \mu_r}\left(\frac{1}{k_y}\frac{\partial E_z}{\partial y} + \psi_{H_{x,y}}\right),\\
\frac{\partial H_y}{\partial t} &= \frac{1}{\mu_0 \mu_r}\left(\frac{1}{k_x}\frac{\partial E_z}{\partial x} + \psi_{H_{y,x}}\right).
\end{aligned} \tag{4}$$

In the above, k_i ($i = x, y$) denotes the wavenumber along the i direction. The notation $\psi_{w,v}$ is defined as $\zeta_w(t) * \partial H_v(t)/\partial w$, where $\zeta_w(t) * \partial H_v(t)/\partial w$ or $\zeta_w(t) * \partial E_v(t)/\partial w$ ($w = x, y$; $v = x, y$) denotes the convolutional term. To reduce the computational time for the calculation of absorption terms $\psi^n_{E_{z,x}}$, $\psi^n_{E_{z,y}}$, $\psi^{n+\frac{1}{2}}_{H_{x,y}}$ and $\psi^{n+\frac{1}{2}}_{H_{y,x}}$, one can approximate them as $\psi^n_{E_{z,x}} = b_x \cdot \psi^{n-1}_{E_{z,x}} + c_x \cdot \frac{\partial H^n_y}{\partial x}$, $\psi^n_{E_{z,y}} = b_y \cdot \psi^{n-1}_{E_{z,y}} + c_y \cdot \frac{\partial H^n_x}{\partial y}$, $\psi^{n+\frac{1}{2}}_{H_{x,y}} = b_y \cdot \psi^{n-\frac{1}{2}}_{H_{x,y}} + c_y \cdot \frac{\partial E^{n+\frac{1}{2}}_z}{\partial y}$, $\psi^{n+\frac{1}{2}}_{H_{y,x}} = b_x \cdot \psi^{n-\frac{1}{2}}_{H_{y,x}} + c_x \cdot \frac{\partial E^{n+\frac{1}{2}}_z}{\partial x}$. Both of the coefficients b_w and c_w take the exponential forms given below

$$\begin{aligned}
b_w &= e^{(-(\frac{\sigma_w}{\epsilon_0 k_w} + \frac{a_w}{\epsilon_0})\Delta t)};\\
c_w &= \frac{\sigma_w}{\sigma_w k_w + k_w^2 a_w}\left(e^{(-(\frac{\sigma_w}{\epsilon_0 k_w} + \frac{a_w}{\epsilon_0})\Delta t)} - 1\right); w = x, y.
\end{aligned} \tag{5}$$

The subscript w denotes x or y and $\sigma_w = \sigma_{max}(\frac{d-w}{d})^m$, $a_w = a_{max}(\frac{d-w}{d})^{m_a}$, $k_w = 1 + (k_{max} - 1) \cdot (\frac{d-w}{d})^m$.

3 Solution algorithm

The equations shown in (4) consist of the ideal Maxwell equations, polarization current term $\underline{J}_d$, and absorption term in the convolutional perfectly matched layer. The quality of simulating EM wave propagation in a dispersive medium characterized by the constitutive equation for the relative electric permittivity ϵ_r depends therefore on the scheme applied to solve Maxwell's equations in free space. The employed constitutive equation is also essential for simulation quality for the polarization current. In addition, the function of the convolutional terms in the CPML equations is to absorb possibly reflected waves from the truncated boundary. The entire set of equations in (4) is therefore decomposed into the ideal Maxwell's equations, the constitutive equation for the Drude medium, the polarization current of the optical medium, and the prescribed wave absorption coefficient in CPML. We need therefore to solve them separately using their respective suitable numerical methods.

Beside the numerical methods employed to calculate the absorption terms $\psi_{H_{x,y}}$, $\psi_{H_{y,x}}$, $\psi_{E_{z,x}}$, and $\psi_{E_{z,y}}$ and the polarization current, the numerical quality of solving the wave equations in Drude medium depends highly on the scheme applied to approximate the following Maxwell's equations in vacuum

$$\begin{aligned}
\frac{\partial E_z}{\partial t} &= \frac{1}{\epsilon_0 \epsilon_r}\left(\frac{1}{k_x}\frac{\partial H_y}{\partial x} - \frac{1}{k_y}\frac{\partial H_x}{\partial y}\right),\\
\frac{\partial H_x}{\partial t} &= -\frac{1}{\mu_0 \mu_r}\left(\frac{1}{k_y}\frac{\partial E_z}{\partial y}\right),\\
\frac{\partial H_y}{\partial t} &= \frac{1}{\mu_0 \mu_r}\left(\frac{1}{k_x}\frac{\partial E_z}{\partial x}\right).
\end{aligned} \tag{6}$$

The necessity of applying a proper temporal discretization scheme is described first in Sect. 4 to preserve symplecitic structure in the above Hamiltonian differential system. One needs also to optimize the dispersion relation equation described in Sect. 5 to approximate the first-order spatial derivative terms. In the current EM wave simulation, our goal is to rigorously determine the users' prescribed values of Δt and $\Delta \underline{x}$. Given the set of independent variables Δt and $\Delta \underline{x}$, we aim to get the corresponding weighting coefficients a_1, a_2 and a_3 in (13) so that the numerical dispersion relation equations for the Ampère's and Faraday's equations can be obtained at all spatial locations of the physical domain.

4 Explicit partitioned Runge-Kutta temporal discretization

In a homogeneous, lossless and sourceless medium, Faraday's and Ampère's equations constitute a Hamiltonian differential system because of the existence of two canonical functions given by $\frac{\partial \underline{E}}{\partial t} = \frac{\delta H}{\partial \underline{H}}$ and $\frac{\partial \underline{H}}{\partial t} = -\frac{\delta H}{\partial \underline{E}}$. For the Maxwell equations investigated in a simple medium, the following Hamiltonian functional H_h exists in the domain Ω [10]

$$H_h(\underline{H}, \underline{E}) = \frac{1}{2}\int_{\Omega}\left(\frac{1}{\epsilon}\underline{H}\cdot\nabla\times\underline{H} + \frac{1}{\mu}\underline{E}\cdot\nabla\times\underline{E}\right)d\Omega. \quad (7)$$

Equations in (6) also conserve the two invariants (or energy densities I and II) given below

$$W_1(t) = \int_{\Omega}(\epsilon\underline{E}\cdot\underline{E} + \mu\underline{H}\cdot\underline{H})\,d\Omega, \quad (8)$$

$$W_2(t) = \int_{\Omega}\left(\epsilon\left|\frac{\partial \underline{E}}{\partial t}\right|^2 + \mu\left|\frac{\partial \underline{H}}{\partial t}\right|^2\right)d\Omega. \quad (9)$$

If one intends to preserve symplectic structure and conserve total energy in the frequency-independent Maxwell's equations, the symplectic scheme of implicit or explicit type should be adopted. In addition to the preservation of symplectic structure along the time direction, we also aim to develop a dispersively more accurate spatial scheme. Our strategy is to derive a scheme with the numerical dispersion relation equation for Maxwell's equations that is equal to its exact dispersion relation equation. The numerical angular frequency shall therefore be derived in terms of the wavenumbers. However, it is difficult to achieve the goal by applying any symplectic-type Runge-Kutta scheme since the resulting formulation involves a coupled set of solution steps to derive the numerical dispersion relation equation. The following explicit symplectic PRK scheme is therefore employed to minimize the difference between the exact and numerical group velocities for the investigated separable Hamiltonian system of TM-mode Maxwell equations

$$\underline{H}^* = \underline{H}^n - \frac{dt}{2\mu}\nabla\times\underline{E}^n, \quad (10)$$

$$\underline{E}^{n+1} = \underline{E}^n + \frac{dt}{\epsilon}\nabla\times\underline{H}^*, \quad (11)$$

$$\underline{H}^{n+1} = \underline{H}^* - \frac{dt}{2\mu}\nabla\times\underline{E}^{n+1}. \quad (12)$$

5 Derivation of the group velocity preserving scheme

The first-order Ampère's and Faraday's equations are first transformed to their respective equivalent second-order equations $\frac{\partial^2 \underline{E}}{\partial t^2} = \frac{1}{\epsilon\mu}\nabla^2\underline{E}$ and $\frac{\partial^2 \underline{H}}{\partial t^2} = \frac{1}{\epsilon\mu}\nabla^2\underline{H}$. Because of these two equations, we shall correctly approximate the semidiscretized Faraday's equation $\underline{H}^* = \underline{H}^n - \frac{dt}{2\mu}\nabla\times\underline{E}^n$ using the centered space scheme for the term $\frac{\partial E_z}{\partial x}$. At the interior point i in a grid system of constant grid spacing Δx, the derivative term $\frac{\partial E_z}{\partial x}$ is approximated by the following equation

$$\left.\frac{\partial E_z}{\partial x}\right|_i = \frac{1}{\Delta x}\big[a_1(E_z|_{i-5/2} - E_z|_{i+5/2}) + a_2(E_z|_{i-3/2} - E_z|_{i+3/2}) + a_3(E_z|_{i-1/2} - E_z|_{i+1/2})\big]. \quad (13)$$

Following the substitution of the above centered approximation equation for $\frac{\partial E_z}{\partial x}|^n$ into Eq. (10) and then the resulting magnetic field solution $\underline{H}^*$ into Eq. (11), the discretized Ampère's equation is derived as follows by virtue of the equations $\underline{H}^n = \underline{H}^0 - \frac{dt}{2\mu}\nabla\times\underline{E}^n$ and $\nabla\times\underline{H}^0 = \frac{\varepsilon}{\Delta t}(\underline{E}^n - \underline{E}^{n-1})$

$$\begin{aligned} E_z|_i^{n+1} = {} & 2E_z|_i^n - E_z|_i^{n-1} \\ & + \frac{c^2\Delta t^2}{\Delta x^2}\big[a_1^2 E_z|_{i-10/2}^n + 2a_1a_2E_z|_{i-8/2}^n \\ & + \big(2a_1a_3 + a_2^2\big)E_z|_{i-6/2}^n \\ & + 2a_3(-a_1 + a_2)E_z|_{i-4/2}^n \\ & + \big(-2a_1a_2 - 2a_2a_3 + a_3^2\big)E_z|_{i-2/2}^n \\ & + \big(-2a_1^2 - 2a_2^2 - 2a_3^2\big)E_z|_i^n \\ & + \big(-2a_1a_2 - 2a_2a_3 + a_3^2\big)E_z|_{i+2/2}^n \\ & + 2a_3(-a_1 + a_2)E_z|_{i+4/2}^n \\ & + \big(2a_1a_3 + a_2^2\big)E_z|_{i+6/2}^n + 2a_1a_2E_z|_{i+8/2}^n \\ & + a_1^2E_z|_{i+10/2}^n\big]. \end{aligned} \quad (14)$$

In the above, $\underline{H}^0$ denotes the calculated value of $\underline{H}$ at $t = (n + \frac{1}{2})\Delta t$. The algebraic equation for Faraday's equation can be similarly derived below using the equations $\underline{H}^n = \underline{H}^0 - \frac{\Delta t}{2\mu}\nabla\times\underline{E}^n$, $\underline{E}^n = \underline{E}^{n-1} + \frac{\Delta t}{\epsilon}\nabla\times\underline{H}^0$ and $\underline{H}^0 = \underline{H}^{n-1} - \frac{\Delta t}{2\mu}\nabla\times\underline{E}^{n-1}$

$$\begin{aligned} H_y|_i^{n+1} = {} & 2H_y|_i^n - H_y|_i^{n-1} \\ & + \frac{c^2\Delta t^2}{\Delta x^2}\big[a_1^2 H_y|_{i-10/2}^n + 2a_1a_2H_y|_{i-8/2}^n \\ & + \big(2a_1a_3 + a_2^2\big)H_y|_{i-6/2}^n \\ & + 2a_3(-a_1 + a_2)H_y|_{i-4/2}^n \\ & + \big(-2a_1a_2 - 2a_2a_3 + a_3^2\big)H_y|_{i-2/2}^n \\ & + \big(-2a_1^2 - 2a_2^2 - 2a_3^2\big)H_y|_i^n \end{aligned}$$

$$+\left(-2a_1a_2-2a_2a_3+a_3^2\right)H_y|_{i+2/2}^n$$
$$+2a_3(-a_1+a_2)H_y|_{i+4/2}^n$$
$$+\left(2a_1a_3+a_2^2\right)H_y|_{i+6/2}^n+2a_1a_2H_y|_{i+8/2}^n$$
$$+a_1^2H_y|_{i+10/2}^n\Big]. \tag{15}$$

The parameters a_1, a_2 and a_3 shown above are to be properly determined to close the algebraic system of the discrete Maxwell's equations.

To get a good overall simulation accuracy, our strategy of determining a_1, a_2 and a_3 is to reduce both of the amplitude and phase errors generated in the approximation of Ampère's and Faraday's equations. The modified equation analysis of second kind is performed first on Eq. (14) or (15) by expanding the terms $\phi_{i\pm5/2}$, $\phi_{i\pm3/2}$ and $\phi_{i\pm1/2}$, where ϕ is E *or* H, in Taylor series with respect to ϕ_i. We eliminate the first two leading discretization errors shown in the derived modified equation. This elimination of error terms enables us to get the following two algebraic equations

$$25a_1^2+9a_2^2+a_3^2+30a_1a_2+10a_1a_3$$
$$+6a_2a_3+5a_1+3a_2+a_3=0, \tag{16}$$

$$1250a_1^2+162a_2^2+2a_3^2+20a_1a_2a_3\left(\frac{102}{a_3}+\frac{13}{a_2}+\frac{3}{a_1}\right)$$
$$+125a_1+27a_2+a_3+2Cr^2(5a_1+3a_2+a_3)=0. \tag{17}$$

In Eq. (17), $Cr(\equiv\frac{c\Delta t}{\Delta x})$ denotes the Courant number (or CFL number), where $c=(\epsilon\mu)^{\frac{1}{2}}$.

One drawback of applying a finite difference method to solve differential equations in the time domain is the association with the accumulated errors stemming from numerical instability, dispersion, while performing anisotropy [11]. In the derivation of the third equation, we perform a Von Neumann stability analysis for ensuring scheme stability, while performing minimization analysis of numerical group velocity error for reducing dispersion and anisotropy errors. In the following, the dispersion analysis will be carried out first. This is done by performing a Fourier stability analysis to determine the free parameters that can render a conditionally stable explicit symplectic scheme. The proposed scheme, having almost zero anisotropy error, will be numerically demonstrated to be applicable to EM wave prediction.

When simulating a wave equation, it is essential to reduce the predicted error in wave speed since it is a function of frequency and propagation angle. Provided that a very small numerical phase or group velocity error is generated, this error may be continuously accumulated and the long-term simulation quality will seriously deteriorate. To get a higher dispersion accuracy, the numerical angular frequency for the differential system of Ampère's and Faraday's equations should correctly relate to the wavenumber. The last required algebraic equation is therefore derived by minimizing the difference between the numerical and exact group velocities. Minimization of dispersive errors starts from transforming the equation in space-time domain (x,t) to its corresponding frequency-wavenumber space (ω,k_x). By substituting the plane-wave solutions $E_z|_i^n=E_z^0e^{I(\omega n\Delta t-k_xi\Delta x)}$ and $H_y|_i^n=H_y^0e^{I(\omega n\Delta t-k_xi\Delta x)}$ into the differential equation (14) or (15), the numerical dispersion relation equation relating the angular frequency ω with the wavenumber k_x

$$\omega_{num}\Delta t=\cos^{-1}\Bigg[\frac{c^2\Delta t^2}{2\Delta x^2}\left(2a_1^2\cos(5k_x\Delta x)\right.$$
$$+4a_1a_2\cos(4k_x\Delta x)$$
$$+2\left(2a_1a_3+a_2^2\right)\cos(3k_x\Delta x)$$
$$+4a_3(-a_1+a_2)\cos(2k_x\Delta x)$$
$$-2\left(-2a_1a_2-2a_2a_3+a_3^2\right)\cos(k_x\Delta x)$$
$$\left.-\left(-2a_1^2-2a_2^2-a_3^2\right)\right)+1\Bigg]. \tag{18}$$

For reducing numerical error of the dispersive type as much as possible, the difference between the exact group velocity $\frac{\partial\omega_{exact}}{\partial k_x}$ and the numerical group velocity $\frac{\partial\omega_{num}}{\partial k_x}$ is minimized in this study. Note that the dispersion relation equation $\omega_{exact}^2=c^2k_x^2$ relates the angular frequency ω_{exact} exactly with the wavenumber k_x in the one-dimensional Maxwell's equations. The error function defined by $[\frac{\partial\omega_{num}}{\partial k_x}-\frac{\partial\omega_{exact}}{\partial k_x}]^2$ is minimized within the integral range $-m\pi\le\gamma\le m\pi$ given below

$$E=\int_{-m\pi}^{m\pi}\left[\frac{\partial\omega_{num}}{\partial k_x}-\frac{\partial\omega_{exact}}{\partial k_x}\right]^2W(\gamma)\,d\gamma. \tag{19}$$

In the above, γ $(=hk_x)$ denotes the scaled wavenumber. Inclusion of the weighting function $W(\gamma)$, which is currently chosen to be the denominator of $[\cdot]^2$, is to make it possible to analytically integrate Eq. (19). By enforcing $\frac{\partial E}{\partial a_3}=0$, we can get a third algebraic equation. This equation derived through the minimization procedure at $m=\frac{1}{2}$, which enables us to get the most accurate result, is used together with the remaining two algebraic equations derived previously by the modified equation analysis of second kind. The resulting introduced coefficients in (13) are $a_1=-0.00805$, $a_2=0.07443$ and $a_3=-1.18302$.

Through the minimization of the dispersive error in wavenumber space and the modified equation analysis for $\frac{\partial H_x}{\partial x}$, the proposed centered difference scheme accommoding the property of yielding the best numerical group velocity is shown to have the spatial accuracy of fourth order since $\frac{\partial H_x}{\partial x}=\frac{\partial H_x}{\partial x}|_{exact}-0.015115\,h^4\frac{\partial^5H_x}{\partial x^5}+O(h^6)+\cdots$.

To get more insight into the dispersive nature of the proposed scheme, the difference between the exact and numerical angular frequencies has been plotted versus wavenumber in [12] at different values of Cr and m. For the proposed scheme, very accurate numerical angular frequency can be obtained for the wavenumber smaller than 1.5. The derived numerical dispersion relation plotted in [12] also shows a better agreement between the exact and numerical group velocity when compared with Yee's scheme.

Derivation of the stability condition for the above proposed explicit scheme starts from scaling the field variables by $\underline{E} = \sqrt{\frac{\mu}{\epsilon}}\underline{E}^*$ or $\underline{H} = \sqrt{\frac{\epsilon}{\mu}}\underline{H}^*$. The set of equations in (6) can then be rewritten as follows for $\underline{V} = \underline{H}^* + I\underline{E}^*$, where I is $(-1)^{1/2}$, in normalized space

$$\frac{1}{\nu}\frac{\partial \underline{V}}{\partial t} = I\nabla \times \underline{V}. \tag{20}$$

It is noted that $\nu = \sqrt{\epsilon\mu}$ and Eq. (20) is valid at $\mu = \epsilon = 1$. The superscript "$*$" is omitted now for the sake of simplicity.

Following the work of Taflove and Brodwin [13], the stability condition will be derived by considering the eigenvalue problem containing the following two equivalent equations

$$\frac{\partial \underline{V}}{\partial t} = \lambda \underline{V}, \tag{21}$$

$$I\nu\nabla \times \underline{V} = \lambda \underline{V}. \tag{22}$$

Equation (21) is approximated by $\underline{V}^{n+\frac{1}{2}} - \underline{V}^{n-\frac{1}{2}} = \lambda\Delta t\underline{V}^n$ using the proposed symplectic time stepping scheme given in Sect. 4. The amplification factor $G(= \frac{\underline{V}^{n+\frac{1}{2}}}{\underline{V}^n})$ can be derived from $G^2 - (\lambda\Delta t)G - 1 = 0$, thereby leading to $G_{1,2} = \frac{\lambda\Delta t}{2} \pm (1 + (\frac{\lambda\Delta t}{2})^2)^{\frac{1}{2}}$. The conditionally stable explicit scheme proposed in this study is found by demanding $\mathrm{Re}(\lambda) = 0$

$$\left|\mathrm{Im}(\lambda)\right| \le \frac{2}{\Delta t}. \tag{23}$$

Substitution of $\frac{\partial \underline{V}}{\partial t} = \lambda\underline{V}$ into Eq. (22) yields $\frac{1}{\nu}\frac{\partial \underline{V}}{\partial t} = I\nabla \times \underline{V}$ or $I\nu(\frac{\partial V_z}{\partial y}) = \lambda V_x$, $I\nu(-\frac{\partial V_z}{\partial x}) = \lambda V_y$ and $I\nu(\frac{\partial V_y}{\partial x} - \frac{\partial V_x}{\partial y}) = \lambda V_z$. These equations can be recast into the matrix form $\underline{\underline{F}}\,\underline{V} = 0$, where

$$\underline{\underline{F}} = \begin{pmatrix} -\lambda & 0 & 2\nu\frac{F_y}{\Delta y} \\ 0 & -\lambda & -2\nu\frac{F_x}{\Delta x} \\ -2\nu\frac{F_y}{\Delta y} & 2\nu\frac{F_x}{\Delta x} & -\lambda \end{pmatrix}. \tag{24}$$

In the above, $F_x = a_1\sin(\frac{5}{2}k_x\Delta x) + a_2\sin(\frac{3}{2}k_x\Delta x) + a_3\sin(\frac{1}{2}k_x\Delta x)$ and $F_y = a_1\sin(\frac{5}{2}k_y\Delta y) + a_2\sin(\frac{3}{2}k_y\Delta y) + a_3\sin(\frac{1}{2}k_y\Delta y)$. One can get the unique solution $\underline{V}$ from the matrix equation $\underline{\underline{F}}\,\underline{V} = \underline{0}$ provided that the determinant of the matrix $\underline{\underline{F}}$ is equal to zero. Calculation of the eigenvalues from $\det(\underline{\underline{F}}) = 0$ leads to $\lambda^2 = -4\nu^2(\frac{F_x^2}{\Delta x^2} + \frac{F_y^2}{\Delta y^2})$. The values of λ for all the possible wavenumbers k_x and k_y exist under

$$\left|\mathrm{Im}(\lambda)\right| \le 2\nu\left(\frac{\max(F_x^2)}{\Delta x^2} + \frac{\max(F_y^2)}{\Delta y^2}\right)^{\frac{1}{2}}. \tag{25}$$

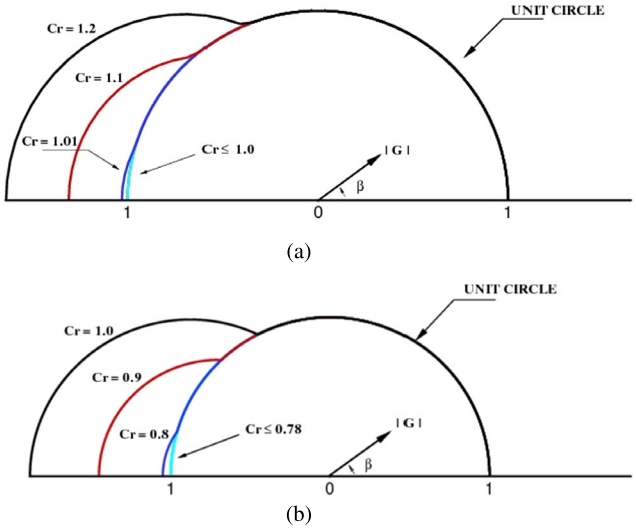

Fig. 1 The amplification factor magnitude $|G|$ is plotted with respect to the modified (or scaled) wavenumber β $(\equiv k_x\Delta x)$ at different values of Cr $(\equiv \frac{c\Delta t}{\Delta x})$ using the Yee's scheme [5] and the proposed numerical group velocity-optimized scheme. (**a**) Yee's scheme; (**b**) proposed scheme

Subject to the constraint equations (23) and (25), the stability equation required to get the convergent solution is given by $\Delta t \le \frac{1}{\nu}(\frac{\max(F_x^2)}{\Delta x^2} + \frac{\max(F_y^2)}{\Delta y^2})^{-\frac{1}{2}}$. By substituting the derived coefficients a_1, a_2 and a_3 into the derived equation for stability sake, one can get the stability conditions for the one-dimensional Maxwell's equations, which is $\Delta t \le 0.78693\frac{\Delta x}{\nu}$, and for the two-dimensional Maxwell's equations, which is $\Delta t \le 0.57095\frac{h}{\nu}$. We can clearly see from Fig. 1 that the Courant number should be smaller than 0.78 to get a stable solution while using the proposed explicit scheme. In comparison with the stability condition of Yee's scheme, which is $0 < Cr < 1$, one needs to use a smaller time step. Our group velocity optimized scheme has, however, a much higher order of accuracy and better phase characteristics as plotted in Fig. 2.

The explicit symplectic PRK scheme developed in staggered grids is verified by solving the TM-mode Maxwell's equations in free space at $\mu = 1$ and $\epsilon = 1$. In this study the TM-mode equation amenable to the analytical solution $E_z(x,t) = \sin(x-t)$ and $H_y(x,t) = -\sin(x-t)$ is solved subject to the initial solenoidal solutions $E_z(x,0) = \sin(x)$ and $H_y(x,0) = -\sin(x)$ in $-2 \le x \le 2$. According to the

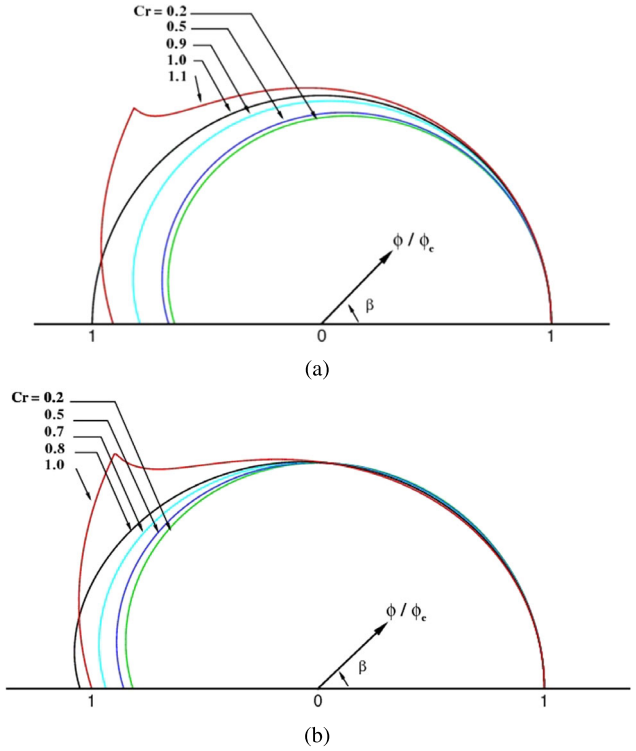

Fig. 2 The predicted relative phase error $\frac{\phi}{\phi_e}$ is plotted with respect to the modified (or scaled) wavenumber β ($\equiv k_x \Delta x$) at different values of Cr ($\equiv \frac{c\Delta t}{\Delta x}$) using the Yee's scheme [5] and the proposed numerical group velocity-optimized scheme. The phase angle ϕ is equal to $\tan^{-1}(\frac{G_i}{G_r})$, where G_r and G_i represent respectively the real and imaginary parts of the amplification factor G. (**a**) Yee's scheme; (**b**) proposed scheme

Table 1 The predicted error norms for E_z and the CPU seconds needed to get the results at $t = 50$ (s). The results are obtained at $Cr = 0.2$ and $m = \frac{1}{2}$

Cr	L_2-error norm	CPU time (s)
0.1	2.7206E-04	9.36E-02
0.2	2.3043E-04	6.24E-02
0.3	8.4952E-04	4.68E-02
0.5	4.7218E-04	3.12E-02
0.7	9.0107E-04	3.12E-02
0.8	Infinity	
0.9	Infinity	

computed error norms tabulated in the Table 1, the proposed scheme with the optimized numerical group velocity in free space for the TM-mode Maxwell's equations is verified. The Hamiltonian defined in (7) and the energy densities I and II in (8–9) plotted with respect to time in Fig. 3 do not change with time. The proposed explicit partitioned Runge-Kutta symplectic scheme is verified to retain the symplectic nature in Maxwell's equations.

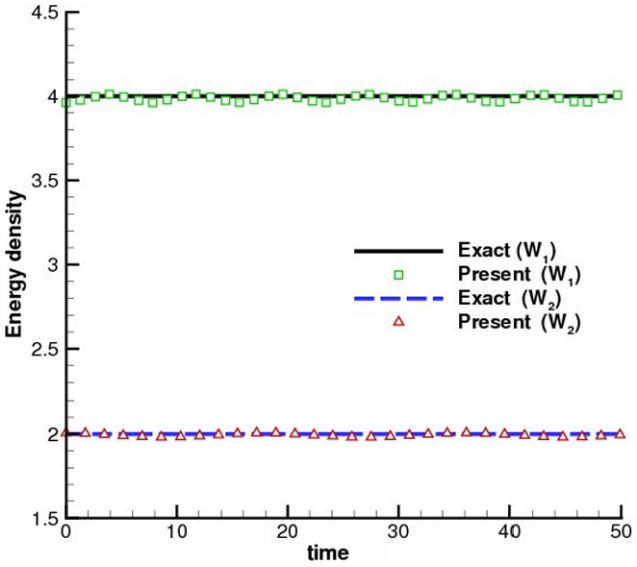

Fig. 3 Comparison of the computed and exact values of W_1 (or the energy density I), shown in (8), and W_2 (or the energy density II), shown in (9), with respect to time

6 Numerical results

Like the motion of electrons in semiconductors, photonic crystals, which are periodic optical nanostructures, can affect also the motion of photons and therefore the propagation of EM waves. In the following, we consider the one-dimensional problem studied previously in [14–16] to learn some of the distinguished features of photonic crystal structures. The problem under investigation has a periodic array containing the alternating thin plasma and dielectric material, or plasma photonic crystals.

The plasma photonic crystal shown in Fig. 4 is composed of alternating thin plasma of width b, dielectric material of width a, and a single defect layer of width c^*. The optical constants used in this study are the same as those used in [14, 15]. In the calculation we consider $\epsilon_1 = 7$ for the non-defect dielectric and $\epsilon_2 = 4.5$ for the defect dielectric. The plasma under current investigation is featured with $\omega_p = 10\pi \times 10^9$ rad/s and $\gamma = 2 \times 10^9$ rad/s. The location of the defect layer is denoted as M and the number of periods of periodic bilayer is N. All the results are computed at $N = 6$, $M = 7$, $a = b = c^* = 1$ cm.

The wave in the frequency range of 0–15 GHz propagates from left to right in an unmagnetized plasma photonic crystal of length 13 cm. For preventing any erroneous wave reflection back to the domain under investigation, ten-layered CPMLs of length 1 mm are attached to both ends of the physical domain. The results obtained at $\Delta t = 2$ ps are used to reveal the effects of N, M, c^* and ϵ_2 on the transmission coefficient (TC)

$$TC(\text{dB}) = 20\ \log_{10}\left[\frac{FFT(total\ field)}{FFT(incident\ field)}\right]. \tag{26}$$

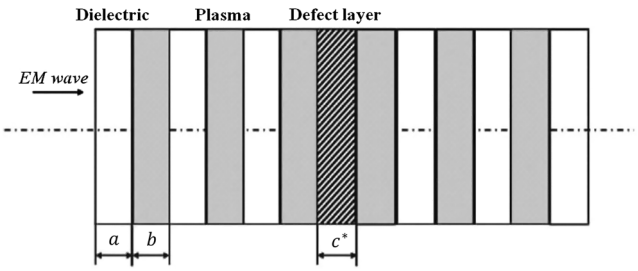

Fig. 4 Schematic of the problem studied in [14] for doped defect layer in the unmagnetic plasma photonic crystal

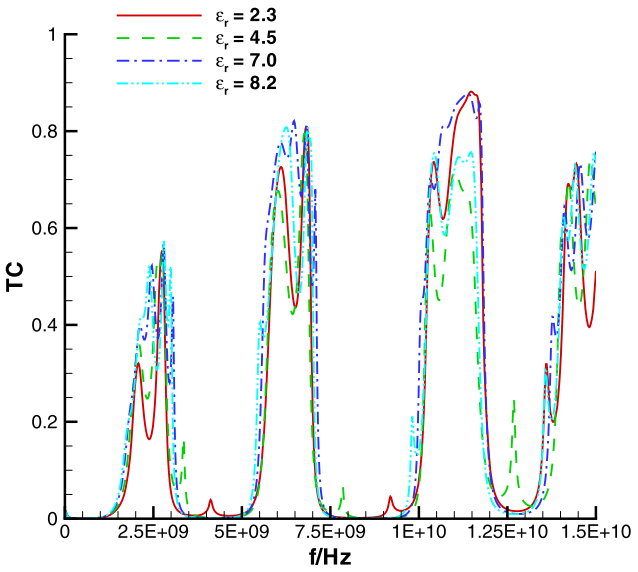

Fig. 5 Comparison of the predicted transmission coefficients (TC) defined in (26) with respect to the incident wave frequencies at different values of the relative permittivity ϵ_r

The dielectric constant of the defect layer has an effect on the wave transmission along the plasma photonic crystal. For this reason, such an effect is studied first by changing the values of ϵ_2, which are 2.3, 4.5, 7 and 8.2.

One can find from the current simulated results in Fig. 5 that the forbidden band width varies slightly. Also, the periodic wave behavior remains almost unchanged in comparison with the computed result without taking the defect layer into consideration. The peak transmission is changed dramatically. At the constant values of $\epsilon_1 = \epsilon_2 = 7$, no defect mode has been observed from the simulated results. Unlike the case free of a defect layer, the simulated defect mode moves toward the direction of a higher frequency when the value of ϵ_2 $(= 2.3$ *or* $4.5)$ becomes smaller than $\epsilon_1 = 7$. On the contrary, when the value of ϵ_2 $(= 8.2)$ is larger than ϵ_1 $(= 7)$ the defect mode is seen to move towards the direction of lower frequency. As the value of ϵ_2 keeps increasing, the transmission coefficient approaches zero with the birth of a defect mode sitting on the left side of the forbidden band. All simulated results plotted in Fig. 5 agree with those predicted earlier in [14].

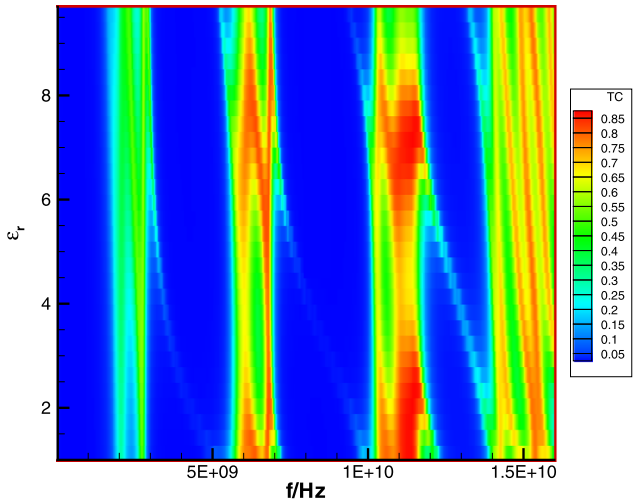

Fig. 6 The contoured values of the relative permittivity ϵ_r are plotted with respect to the frequencies of incident wave

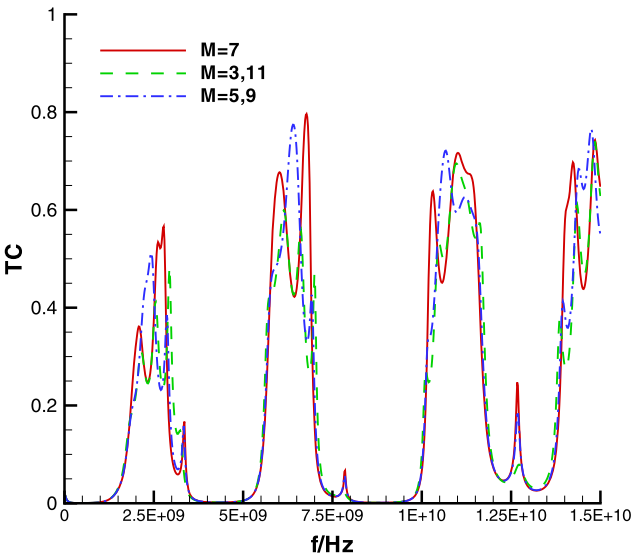

Fig. 7 Comparison of the simulated transmission coefficients (TC) with respect to the incident wave frequencies at different values of M

For a better understanding of the effect of ϵ_2 $(1 < \epsilon_2 \leq 10)$ on the wave propagation in plasma photonic crystal, we plot the value of relative permittivity in Fig. 6 with respect to frequency. The simulated defect modes are almost periodically distributed regardless of the value of ϵ_2. The effects of the defect layer location and the number of periods of the periodic bilayer on the wave propagation along the plasma photonic crystal are also investigated. We investigate first the effect of defect layer locations by adding a defect layer respectively at $M = 3, 5, 7, 9$ and 11. In Fig. 7, all the defect modes are seen to occur in the same frequency range regardless of the defect layer location. Similar

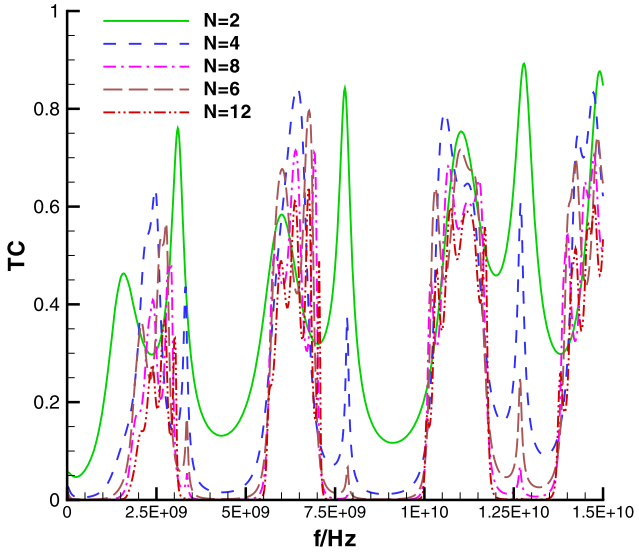

Fig. 8 Comparison of the simulated transmission coefficients (TC) with respect to the incident wave frequencies at different values of N

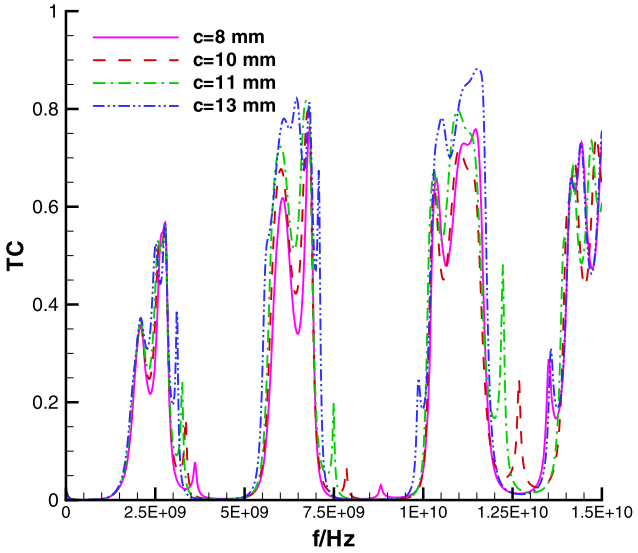

Fig. 9 Comparison of the simulated transmission coefficients (TC) with respect to the incident wave frequencies at different values of a single defect layer of width c^* shown in Fig. 4

to the predicted result in [14], the peak transmission coefficient increases as the defect layer is located at a point located closer to the center of the photonic crystal. The doped defect layer is therefore known to have a greater impact (or destruction) on the photonic crystal when its location is closer to the crystal center. The predicted peak around 12.5 GHz is larger than the magnitude of 11.25 GHz predicted in [14].

Discussion of the results is followed by changing the values of N $(= 2, 4, 6, 8, 12)$ to investigate the effect of the number of periods in the plasma photonic crystal. At the smallest value of $N = 2$, both of the forbidden band and the defect mode are not clearly observed. As N is larger than 4, forbidden bands become clearly observed in the predicted results shown in Fig. 8. With increasing values of N, the number of peaks in the transmission coefficient increases to two. The range of the defect mode frequency remains however almost unchanged regardless of the values of N. The physical reason for these predicted results is due mainly to the interaction between the EM waves and the reflection waves resulting from the defect layer. As the value of N increases, the peak transmission coefficient decreases accordingly because of the dissipative nature and the larger plasma absorption coefficient.

The defect layer width is also taken into account by changing the values of c^* (which are 8, 10, 11, 13 and 38 mm). According to Fig. 9, one can observe from the predicted results that the frequency range of the defect mode shifts towards the direction of a higher frequency as the defect layer width becomes smaller. On the contrary, the increased defect layer width results in a shift of the defect mode directing towards a lower frequency. As the width becomes large enough, no wave is permitted to pass through

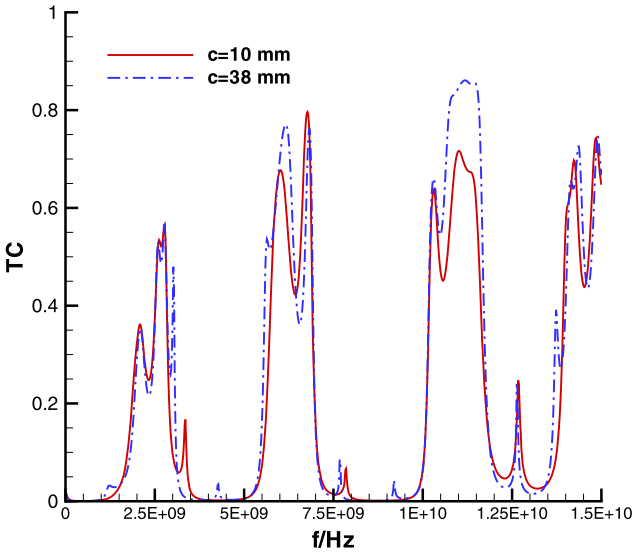

Fig. 10 Comparison of the simulated transmission coefficients (TC) with respect to the incident wave frequencies at two different values of c^* shown in Fig. 4

the photonic crystal. Under the circumstances, a newly born defect mode becomes visible and takes its position on the left side of the forbidden band. As the width of the defect layer keeps increasing to 38 mm, one newly born defect mode appears, as shown in Fig. 10. Such an increase of the defect mode is due possibly to the enhanced interaction between the propagation wave along the positive direction and the wave reflected from the defect layer. A decreasing defect mode frequency and an increasing interferenced wavelength therefore result.

7 Concluding remarks

A finite difference scheme is rigorously developed to simulate Maxwell's equations in the frequency-dependent Drude medium. Our aim is to preserve the symplectic property in the ideal Maxwell equations. Also, we aim to optimize the numerical group velocity in free space. The results obtained from the proposed explicit symplectic PRK method in Drude medium agree excellently with the analytical result. The effect of the defect mode in unmagnetized plasma photonic crystals is then investigated using the proposed symplecticity and group-velocity preserving scheme.

References

1. Nicolaides, R.A., Wang, D.Q.: Helicity and variational principles for Maxwell's equations. Int. J. Electron. **54**, 861–864 (1983)
2. Cockburn, B., Li, F., Chi, C.W.: Locally divergence-free discontinuous Galerkin methods for the Maxwell equations. J. Comput. Phys. **194**(2), 588–610 (2004)
3. Sheu, W.H., Hung, Y.W., Tsai, M.H., Chiu, P.H., Li, J.H.: On the development of a triple-preserving Maxwell's equations solver in non-staggered grids. Int. J. Numer. Methods Fluids **63**, 1328–1346 (2010)
4. Sheu, W.H., Liang, L.Y., Li, J.H.: Development of an explicit symplectic scheme that optimizes the dispersion-relation equation of the Maxwell's equations. Commun. Comput. Phys. **13**(4), 1107–1133 (2013)
5. Yee, K.S.: Numerical solution of initial boundary value problem involving Maxwell's equations in isotropic meida. IEEE Trans. Antennas Propag. **4**(3), 302–307 (1966)
6. Roden, J.A., Gedney, S.D.: Convolutional PML (CPML): an efficient FDTD implementation of the CFS-PML for arbitrary media. Microw. Opt. Technol. Lett. **27**, 334–339 (2000)
7. Zheng, F., Chen, Z., Zhang, J.: An FDTD method without the Courant stability conditions. IEEE Microw. Guided Wave Lett. **9**(11), 441–443 (1999)
8. Sun, G., Trueman, C.: Efficient implementations of the Crank-Nicolson scheme for the FDTD method. IEEE Trans. Microw. Theory Tech. **54**(5), 2275–2284 (2006)
9. Kantartzis, N.V., Tsiboukis, T.D.: Modern EMC Analysis Techniques: Models and Applications. Morgan and Claypool, San Rafael (2008)
10. Anderson, N., Arthurs, A.M.: Helicity and variational principles for Maxwell's equations. Int. J. Electron. **54**, 861–864 (1983)
11. Sha, W., Hunag, Z., Chen, M.S., Wu, X.L.: Survey on symplectic finite-difference time-domain scheme for Maxwell's equations. IEEE Trans. Antennas Propag. **56**, 493–500 (2008)
12. Sheu, W.H., Chung, R.Y., Li, J.H.: Development of a symplectic scheme with optimized numerical dispersion-relation equation to solve Maxwell's equations in dispersive media. Prog. Electromagn. Res. **132**, 517–549 (2012)
13. Taflove, A., Brodwin, M.E.: Numerical solution of steady-state electromagnetic scattering problems using the time-dependent Maxwell's equations. IEEE Trans. Microw. Theory Tech. **23**, 623–630 (1975)
14. Ma, L., Zhang, H.F., Liu, S.B.: Study on the defect mode properties of magnetized plasma photonic crystals. Acta Phys. Sin. **57**(8), 5089–5094 (2008)
15. Zhang, H.F., Ma, L., Liu, S.B.: Defect mode properties of magnetized plasma photonic crystals. Acta Phys. Sin. **58**(2), 1071–1076 (2009)
16. Liu, S., Zhong, S.Y., Liu, S.Q.: A study of properties of the photonic band gap of unmagnetized plasma photonic crystal. Plasma Sci. Technol. **11**(1) (2009)